21st Australasian Fluid Mechanics Conference
Adelaide, Australia
10-13 December 2018

Linear Stability Analysis and Direct Numerical Simulations of Swirling Buoyant Flows

J. Singh[1], **H. M. Blackburn**[1], **J. M. Lopez**[2], **A. J. Smits**[3]

[1]Department of Mechanical and Aerospace Engineering
Monash University, Victoria 3800, Australia

[2]School of Mathematical and Statistical Sciences
Arizona State University, Tempe, AZ 85287, USA

[3] Department of Mechanical and Aerospace Engineering
Princeton University, NJ 08540, USA

Abstract

The current study investigates the effect of heating defined via Richardson number on the stability of swirling flows via linear stability analysis and direct numerical simulations. Such flows are common in combustion and mixing applications and are simple models for atmospheric flows such as fire whirls and dust devils. The linear stability characteristics of azimuthal wavenumbers $m = 1$-5 are investigated at a fixed Reynolds number of 500 and at three inlet swirl angles where the non-buoyant (without heating) flow shows linear stability characteristics different from each other. The results show that the heating may initially have a stabilising effect but with more heating, the flow ultimately becomes unstable to perturbations. The growth rate of the leading eigenmode agrees with the predictions of three-dimensional direct numerical simulations. The centre-line axial velocity is increased noticeably with heating, indicating much larger axial momentum in unstable buoyant flows than non-buoyant flows.

Introduction

Plume flows with swirl entry are common in applications such as in combustion and mixing and are the simplest models for atmospheric swirling flows – fire whirls and dust devils. Fire whirls and dust devils share similarities such as they require a background circulation and they harvest energy from the buoyancy generated due to a localised heating near the ground. In addition to the energy source, an eddy generating mechanism is also essential for the formation of dust devils and fire whirls [9]. Eddies may be generated by the topographical features, via the interaction of multiple flames or by the interaction of the flame with the local shear and ambient conditions [5, 9]. Under favourable conditions, they can extend hundreds of meters above the ground. In case of combustion applications, swirling flows provide improved combustion characteristics and fuel efficiency. Despite their applications and importance, the basic fluid dynamics of these flows is poorly understood.

Fire whirls and dust devils have been studied via field observations, however, much insight into their flow has been gained via laboratory experiments. Laboratory experiments of fire whirls have shown longer flames with rotation imposed compared to non-rotating flames, which is primarily due to the suppression of turbulence by rotation. In the case of pool fires, additional flame lengthening occurs due to increased convection, which increases fuel burning [4]. The azimuthal velocity in a fire whirl showed a radial distribution similar to a forced vortex inside the core region and a free vortex outside the core [4].

The present study uses direct numerical simulations and global stability analysis to systematically investigate the effect of buoyancy and circulation on a plume flow with a tangential entry with the primary objective of investigating the stability of

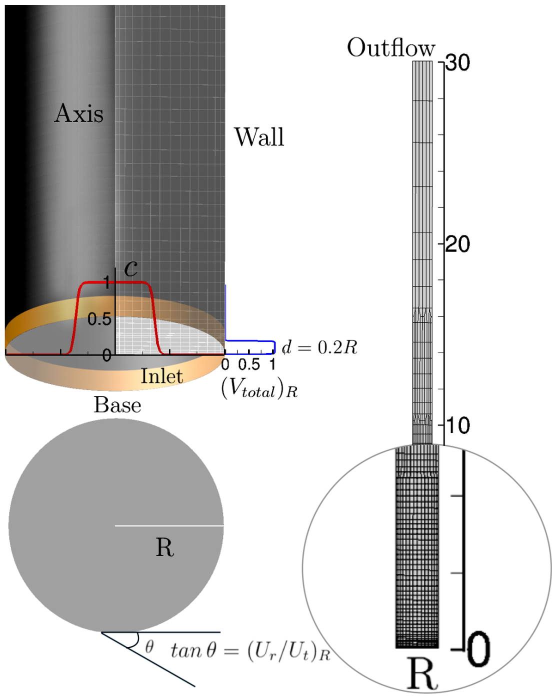

Figure 1: Schematic of the computational domain. The red curve shows the imposed scalar distribution at the base and the blue curve shows the profile of the velocity magnitude imposed at the inlet. The image on the right shows the full domain with a closer look of the mesh near the base; domain's vertical height is 30R.

the flow. Our simulation model is a cylindrical domain of radius R with a heated base and outflow at the top (figure 1). The flow with a specified velocity vector and temperature enters through the side wall. The inlet swirl angle θ is defined as $\tan\theta = U_r/U_t$, where U_r is the inlet radial velocity and U_t is the inlet tangential velocity. The past experimental studies of laboratory scale fire whirls showed that most of the inflow occurs near the ground [7], therefore, we restrict the inlet height to $d = 0.2R$. The total inflow entering into the domain is fixed, which implies lower swirl and higher radial inlet velocities at larger θ. The average inlet velocity U_0 is used for the velocity scaling and the radius of the domain R is used for the length scale. In an unpublished separate study we obtained the neutral stability curves for different azimuthal wavenumbers in non-buoyant swirling flows (figure 2) using the same methodology as used here. In the current study, the effect of heating is investigated at a fixed Reynolds number, $Re = 2U_0R/\nu = 500$ where ν is the fluid's kinematic viscosity. The effect of heating is quantified via Richardson number Ri defined as:

$$Ri = g\beta(c_s - c_0)R/U_0^2. \quad (1)$$

Here, g is the gravitational acceleration, c_s is the base temperature, c_0 is the ambient temperature and β is the coefficient of thermal expansion which is taken as $1/c_0$ for air. The radius of the heated region on the base is $R_h \approx 0.25R$. Three swirl angles are considered, $\theta = 40^\circ$, 50° and 60°. As seen in figure 2, the non-buoyant flow shows different linear stability characteristics at these swirl angles; the flow is linearly stable for $\theta = 40^\circ$ and unstable for azimuthal wavenumber $m = 2$ at $\theta = 50^\circ$ and for $m = 1$ at $\theta = 60^\circ$. The current numerical set-up mimics the fire tornado simulator at the Singapore science centre and is similar to the one used by Wang et al. [10] for non-buoyant flows.

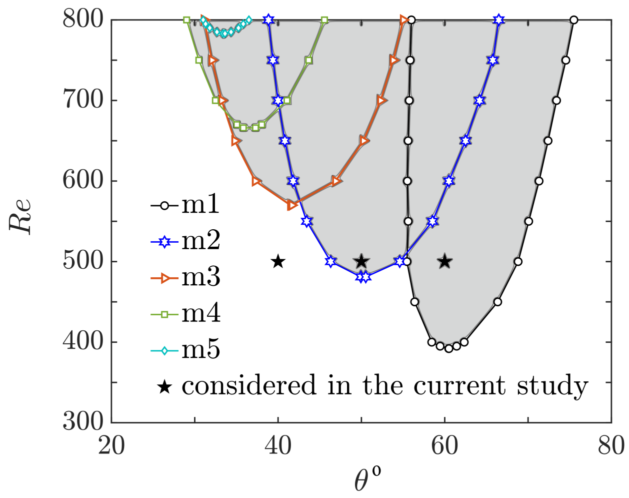

Figure 2: Neutral stability curves for different azimuthal wavenumbers estimated using the linear stability analysis of non-buoyant swirling flows. Unstable region is shown in grey. Points marked by (★) are analysed in the current study for the effect of buoyancy.

Methodology

We use a spectral element-Fourier code [2] to solve the following non-dimensional continuity, momentum and energy equations:

$$\nabla \cdot \boldsymbol{v} = 0 \quad (2)$$

$$\partial \boldsymbol{v}/\partial t + \boldsymbol{v} \cdot \nabla \boldsymbol{v} = -\nabla p + 2Re^{-1}\nabla^2 \boldsymbol{v} - \hat{\imath} Ri c \quad (3)$$

$$\partial c/\partial t + \boldsymbol{v} \cdot \nabla c = 2(RePr)^{-1}\nabla^2 c \quad (4)$$

where $\hat{\imath}$ denotes the axial direction, $\boldsymbol{v}$ is the velocity vector, p is the pressure, Pr is the prandtl number and c is the non-dimensional temperature defined as $c = (c' - c_0)/(c_s - c_0)$ where c' is the dimensional temperature; thus, c varies from 0 to 1. The Boussinesq approximation is used for modelling the buoyancy, therefore, the fluid properties are assumed constant. The energy equation is coupled to the momentum equation via the buoyancy term Ric. The nature of convection (natural or forced) is usually dependent on the Richardson number with natural convection being negligible for $Ri < 0.1$ and forced convection being negligible for $Ri > 10$. For $0.1 < Ri < 10.0$, neither of the convections can be neglected. Fire whirls can be approximately 1m-3 km in diameter with wind speeds of 10-50 m s^{-1} and the core temperature up to 1000° C [9]. For these values, the Richardson number Ri varies from less than 0.1 to more than a hundred.

The inlet velocity smoothly transitions from zero to the maximum value at both sides of the inlet. Similarly, a smooth transition for c at the base is ensured from $c = 1$ for $r < R_h$ to $c = 0$ for $r > R_h$ where r is the radial distance (see figure 1). The non-dimensional temperature at the wall and at the inlet is set to 0 (ambient temperature). A no-slip boundary condition is used for the velocity at the base and at the wall and a robust outflow boundary condition due to Dong et al.[3] is used at the outflow. The governing equations are solved in cylindrical coordinates where the radial-axial plane is discretized using spectral elements and Fourier expansions are used in the periodic azimuthal direction. Since we are interested in the flow dynamics near the base, a finer mesh-resolution is used there and the mesh is sequentially coarsened towards the outlet (see the right panel in figure 1). The mesh used in three-dimensional DNS had 978 spectral elements of polynomial order 7 and 96 azimuthal planes.

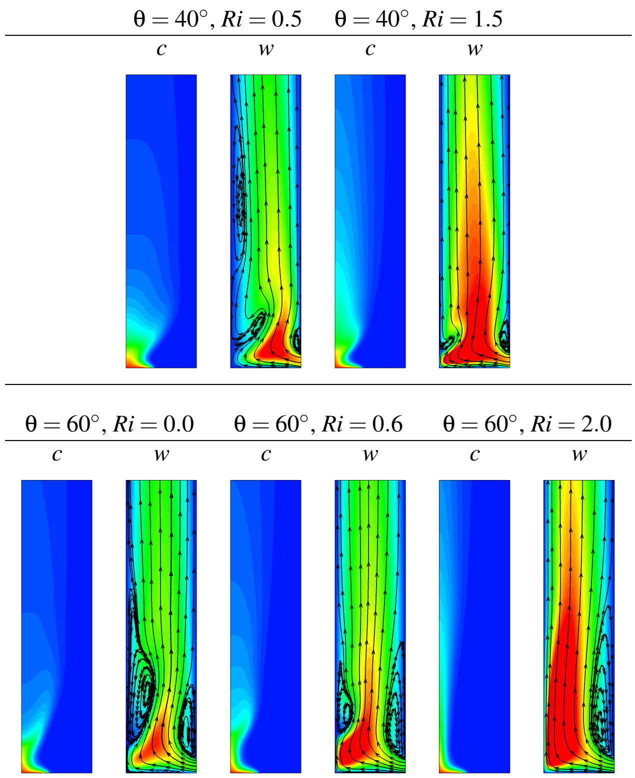

Figure 3: Base flow for different swirl angles θ and Ri. Contours are shown for scalar c and the azimuthal velocity w and streamlines are plotted for radial-axial velocities. Contours levels (blue to red) are in the range $0 - 1$ for c and $0 - 1.5$ for w. In all panels, the horizontal axis varies from 0 to R the vertical extent is $x = 4R$.

For the linear stability analysis, base flows are generated using the same numerical set-up as explained above but using only one azimuthal plane (two-dimensional). Simulations were run until the flow reaches a steady state following which the linear stability computations are carried out for azimuthal wavenumbers $m = 0 - 5$. An eigenvalue solver is used for the linear stability analysis, which solves eigensystem iteratively by using an orthogonal projection of the linear operator onto a Krylov subspace. For more details of the linear stability code we refer to reader to [1, 8].

Results and discussion

Linear stability analysis

The distribution of the temperature and the velocity in the base flow is shown in figure 3 for $\theta = 40°$ and $60°$ at different Ri. Larger azimuthal velocities are evident for both θ in buoyant flows ($Ri > 0$) compared to non-buoyant ones ($Ri = 0$). The non-buoyant flows show two regions of reversed axial flow, one near the domain axis and the other near the wall. The near-axis vortex shrinks whereas the near-wall vortex grows in size as Ri is increased from 0.0 to 1.5 for $\theta = 40°$. The same is observed for $\theta = 60°$ and the near-axis vortex disappears for $Ri = 2.0$. As the near-axis vortex shrinks with increasing Ri, the higher temperature region shifts towards the domain axis. The larger radial momentum of the inflow in $\theta = 60°$ compared to $\theta = 40°$ also helps in concentrating the high temperature region near the axis.

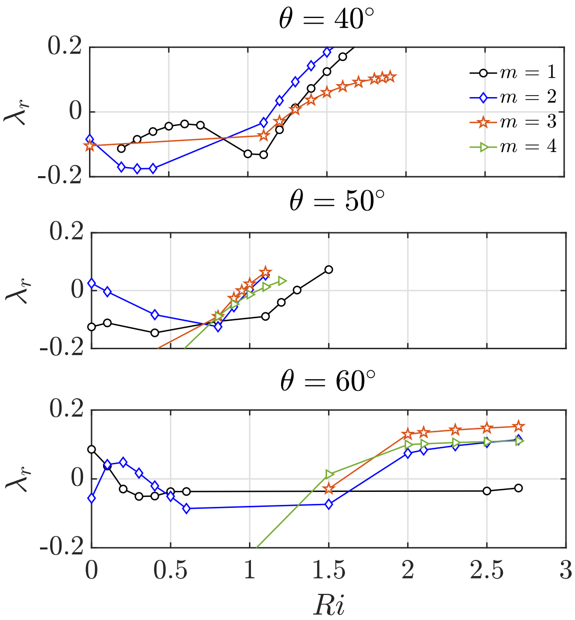

Figure 4: Growth rates from the linear stability analysis for three swirl angles at $Re = 500$ plotted as a function of Ri. Only the results of azimuthal wavenumbers which becomes unstable in the range of Ri considered are shown.

Figure 4 shows the growth rates λ_r (the real part of the eigenvalue) from the eigenvalue solver plotted for different θ as a function of Ri. In each panel, only the results of azimuthal wavenumbers which become unstable in the range of Ri investigated are included. At $\theta = 40°$ where the non-buoyant is stable ($\lambda_r < 0$) remains stable until Ri reaches to 1.0 and become unstable ($\lambda_r > 0$) thereafter for azimuthal wavenumbers $m = 1-3$. The azimuthal wavenumber $m = 2$ become unstable first followed by $m = 1$ and $m = 3$ with increasing Ri. The eigenmode shapes plotted in figure 5 show that different azimuthal wavenumbers become unstable in different regions of the domain. The higher azimuthal wavenumber i.e. $m = 3$ appears near the wall and close to the base whereas $m = 2$ appears near the centre of the domain, and $m = 1$ appears near the domain axis and away from the base. In contrast to $\theta = 40°$, the non-buoyant flow ($Ri = 0.0$) is unstable for other swirl angles. As seen in figure 4, the linear growth rates show a distinct behaviour for $\theta = 50°$ and $\theta = 60°$ with increasing Ri. At $\theta = 50°$ for which, the azimuthal wavenumber $m = 2$ was unstable in non-buoyant flow becomes quickly stable with adding buoyancy; however, it along with wavenumbers $m = 3, 4$ become unstable for $Ri \gtrsim 1.0$.

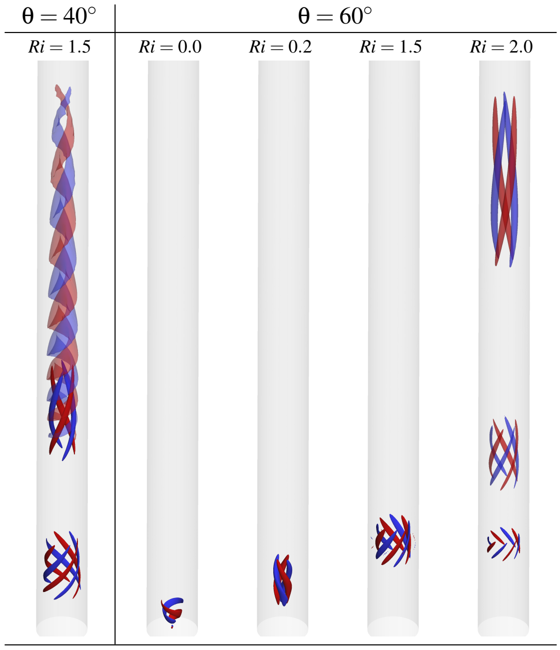

Figure 5: Eigenmode shapes of different azimuthal wavenumbers visualised via the iso-surfaces of axial vorticity; red is positive and blue is negative. The domain vertical extent shown is $30R$ (full domain).

In contrast to $\theta = 50°$, the flow with $\theta = 60°$ does not immediately become stable with addition of buoyancy. Although, buoyancy stabilises the non-buoyant unstable wavenumber $m = 1$, $m = 2$ becomes unstable returning to the stability again as Ri reaches ≈ 0.4. With further increasing Ri, the azimuthal wavenumber $m = 4$ first becomes unstable followed by $m = 3$ and $m = 2$. In the range of Ri considered, neither of $m = 1$ and $m = 5$ show a positive linear growth rate and thus, remain linearly stable to perturbations. Similar to $\theta = 40°$, higher azimuthal wavenumbers become unstable close to the base and away from the domain axis compared to lower azimuthal wavenumbers (figure 5). The azimuthal wavenumber $m = 2$ is concentrated near the axis and is axially stretched in buoyant flow compared to the non-buoyant flow.

Overall, these results show that the buoyancy has both stabilising and non-stabilising effects depending on the nature of the non-buoyant flow and the inlet swirl angle θ. It stabilises the non-buoyant unstable azimuthal wavenumbers but the instabilities may appear in other wavenumbers. For all swirl angles considered here, the flow ultimately becomes unstable with increasing Ri.

Direct numerical simulations

Three-dimensional DNS are carried out to verify the linear stability results using the initial conditions generated by adding the leading unstable eigenmode to the base flow. The iso-surfaces of axial vorticity and the temperature are shown in figure 6 for $\theta = 40°$ and $\theta = 50°$ at different Ri. The near-axis region (core) is dominated by the positive vorticity and negative vorticity wraps around the positive vorticity. As expected from the linear stability analysis, the flow is axi-symmetric for $Ri < 1.0$ for both θ but twisting of the positive vorticity iso-surface and breaking down of the negative iso-surface is seen for $Ri = 1.5$ for both θ. Energy in the leading Fourier mode for these cases

($Ri = 1.5$) initially grows exponentially at a rate expected from the linear stability analysis then diverts below to a constant energy value (not shown here), which indicates the super-critical non-linear behaviour of the bifurcation.

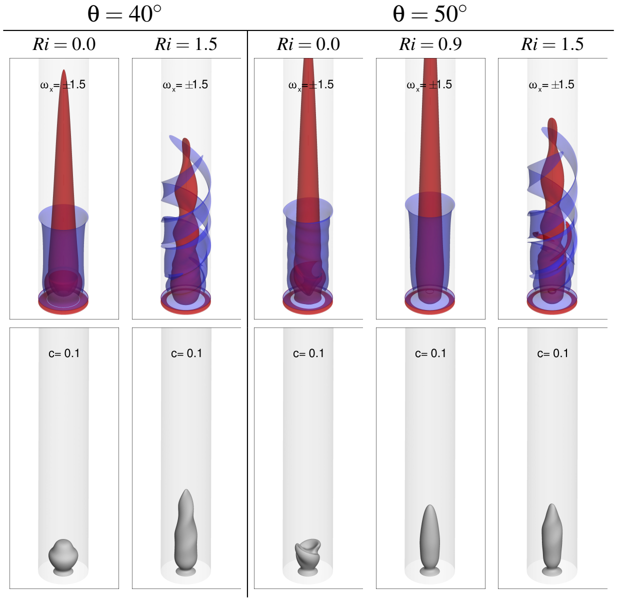

Figure 6: Top row shows iso-surfaces of axial vorticity for $\theta = 40^\circ$ and 50° at different Ri from DNS. Red shows the positive vorticity and blue shows the negative vorticity. The bottom row shows the iso-surfaces of the non-dimensional temperature for the corresponding cases. Vertical extent is $x \approx 10R$ in all panels.

Once the energy in different Fourier modes reach to steady value, statistics are collected for a thousand simulation time units which corresponds to approximately thirty flow-through times. The time-averaged profiles of the centre-line non-dimensional temperature and axial velocity are shown in figure 7 for non-buoyant ($Ri = 0.0$) and unstable buoyant ($Ri = 1.5$) flows at $\theta = 40^\circ$ and $\theta = 50^\circ$. With heating, the axial velocity is significantly enhanced. The maximum velocity is approximately seven times larger for more swirling flow ($v_{t_R} > v_{r_R}$ in $\theta = 40^\circ$) and approximately four times larger for less swirling flow ($v_{t_R} < v_{r_R}$, $\theta = 50^\circ$) in buoyant flow compared to non-buoyant flow. The location of the peak value is slightly closer to the axis for $\theta = 40^\circ$ whereas is slightly away from the axis for $\theta = 50^\circ$ in buoyant flow compared to non-buoyant flow. Overall the DNS results are consistent with the linear stability predictions and highlight the differences between more swirling and less swirling flows and buoyant and non-buoyant flows.

Conclusions

The current study employs direct numerical simulations and the linear stability analysis to investigate the effect of buoyancy on the stability of swirling flows. The Reynolds number is fixed and three swirl angles of distinct non-buoyant linear stability nature are considered. The results show that the buoyancy initially has a stabilising effect on the unstable non-buoyant azimuthal wavenumbers, however, the flow ultimately becomes unstable to different azimuthal wavenumbers with heating although at different Ri depending on θ and the azimuthal wavenumber. The three-dimensional DNS predictions of the growth rate of the leading eigenmode agree with the linear stability predictions. The time-averaged centre-line axial velocity is significantly increased with buoyancy, which suggests a significantly larger axial momentum in buoyant flows compared to non-buoyant ones.

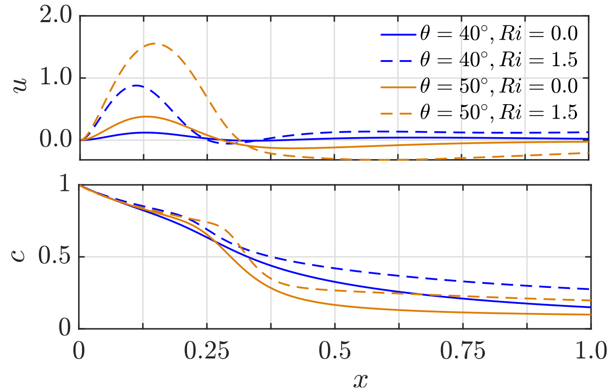

Figure 7: Non-dimensional temperature (top) and axial velocity (bottom) plotted as a function of height x for $\theta = 40^\circ$ and $\theta = 50^\circ$ at different Ri.

Acknowledgements

The authors acknowledge the computational resources provided by Pawsey under the grant D77. The current study was supported by the ARC grant DP160103961.

References

[1] Barkley, D., Blackburn, H. M. and Sherwin, S. J., Direct optimal growth analysis for timesteppers, *International journal for numerical methods in fluids*, **57**, 2008, 1435–1458.

[2] Blackburn, H. M. and Sherwin, S. J., Formulation of a Galerkin spectral element–Fourier method for three-dimensional incompressible flows in cylindrical geometries, *J. Comput. Phys.*, **197**, 2004, 759–778.

[3] Dong, S., Karniadakis, G. E. and Chryssostomidis, C., A robust and accurate outflow boundary condition for incompressible flow simulations on severely-truncated unbounded domains, *J. Comput. Phys.*, **261**, 2014, 83–105.

[4] Emmons, H. W. and Ying, S.-J., The fire whirl, in *Symp. (Int.) on Comb.*, Elsevier, 1967, volume 11, 475–488, 475–488.

[5] Forthofer, J. M. and Goodrick, S. L., Review of vortices in wildland fire, *J. Comb.*, **2011**.

[6] Goens, D. W., Fire whirls, Technical report, NOAA Technical Memorandum NWS WR-129, Missoula, Montana, 1978.

[7] Hartl, K., *Experimental Investigation of Laboratory Fire Whirls*, Ph.D. thesis, Princeton Univ., 2016.

[8] Pitz, D. B., Marxen, O. and Chew, J. W., Onset of convection induced by centrifugal buoyancy in a rotating cavity, *J. Fluid Mech.*, **826**, 2017, 484–502.

[9] Tohidi, A., Gollner, M. J. and Xiao, H., Fire whirls, *Annu. Rev. Fluid Mech.*, **50**, 2018, 187–213.

[10] Wang, Y., Wang, X. and Yang, V., Evolution and transition mechanisms of internal swirling flows with tangential entry, *Phys. Fluids*, **30**, 2018, 013601.